Low-temperature synthesis and characterization of PVP-capped FeAu nanoparticles

HongLing Liu and Peng Hou
Institute of Molecular and Crystal Engineering, School of Chemistry and Chemical Engineering, Henan University, Kaifeng 475004, China

JunHua Wu[a)]
Pioneer Research Center for Biomedical Nanocrystals, Korea University, Seoul 136-713, Korea

(Received 28 February 2011; accepted 2 May 2011)

We report the low-temperature synthesis and characterization of polyvinylpyrrolidone (PVP)-capped FeAu magneto-plasmonic multifunctional nanoparticles by a one-step nanoemulsion process. The Fourier transform infrared spectroscopy study proves the PVP coating on the surface of the resultant FeAu nanoparticles, whereas the structural, magnetic, and optical analysis illustrates the fusion of iron and gold into one single nanostructure showing the nanoparticle shape and a tight size distribution with an average size of 11.3 nm, followed by the growth habit compared to other relevant nanoparticles. Moreover, the PVP-capped FeAu nanoparticles manifest soft ferromagnetic behavior with a small coercivity of ~40 Oe at room temperature. The corresponding magnetic hysteresis curves were elucidated by modified bi-phase Langevin equations, which were reasonably interpreted with the binary particle size distribution. The nanoparticles reveal a well-defined surface plasmon resonance band at ~546 nm and a visual demonstration shows the magnetic separability of all nanoparticles for potential magnetic and/or optical manipulation.

I. INTRODUCTION

Nanoparticles of multiple constituents have gained a prominent momentum in the interdisciplinary convergence of biology and medicine with physical sciences and nanotechnology, in view of prospective application and fundamental challenge in many areas such as multifunctional nano-carriers and nanoscale building blocks.[1–7] In particular, bimetallic alloy nanoparticles are fascinating nanostructured materials attributed to their special structure and properties and have found widespread use in chemical detection, biological sensing, catalysis, photoelectronic devices, medicine, and information storage. In binary candidates, two elements, iron and gold, are of great significance in constructing such binary nanostructures.[8] Physicochemically, iron is an excellent material owing to its high magnetization and easy conversion to biocompatible oxides, which have been thoroughly studied in the form of magnetic nanoparticles in the biomedical field.[9,10] In fact, the binary nanoparticles containing Fe have been mostly investigated in consideration of unique properties other than their bulk counterparts resulting from reduced dimension.[11–13] On the contrary, gold shows attractive optical properties, biological compatibility, catalytic activity, and excellent surface effects.[14–16] Uniquely, nanostructured gold reveals a strong absorption band in the visible region as a result of surface plasmon, which is defined by the particle size and the physicochemical environment surrounding the nano-entity. The phenomenon has been used in biomolecular colorimetry with high selectivity, whereas the exceptional Au surface, benign to the living body, is targeted for versatile surface chemistry that renders sites available for firm bonding with biomolecules through mercapto groups.[3,14,17,18] Recognizing the peculiar optical properties and surface chemistry, extensive researches have been carried out to prepare Au binary alloy nanostructures with another element other than iron.[19–23]

Interest has surged recently, circumventing the phase separation of the elements on the macroscopic scale which happens over almost all the composition under ambient conditions,[24,25] to produce binary iron–gold (FeAu) nanoparticles to incorporate the magnetic and optical functioning in one single entity and to simultaneously tackle the two issues of surface modification and biocompatibility for biomedical purposes.[8,26–31] Reasonably, the synthesis of FeAu alloy nanoparticles is constructively important in taking advantages of both magnetic and optical properties in addition to the biological compatibility and easy linking to biomolecules offered by the compositions. Thus, it is foreseen that amalgamation of these two elements into a single block on the nanoscale should produce a new nanostructured material which retains the optical and magnetic properties of the respective components, synergistically proffering enhanced performance and functionalities which go beyond

[a)]Address all correspondence to this author.
e-mail: feitianshenhu@yahoo.com
DOI: 10.1557/jmr.2011.161

 © Materials Research Society 2011

https://doi.org/10.1557/jmr.2011.161 Published online by Cambridge University Press

those of the individual components.[8,26–31] As the binary nanoparticle system is still far away from being thoroughly investigated, new synthesis of such nanoparticles, particularly, nontoxic approaches and proper surface tailoring, is a useful expansion of the field.

Moreover, smart, functional, and bio-friendly polymers have drawn growing scientific attention as a result of their diverse potential applications such as tunable delivery vehicles, biomineralization templating, and scaffolds for biological conjugation. In addition, the use of a biocompatible polymer can meet the demands on a green synthesis process with respect to environmental concern and natural coating of nanoparticle surfaces by biocompatible molecules for desired applications in life sciences. We are interested in using such polymers as nanoreactors to fabricate a range of multifunctional nanoparticles for potential applications in biomedicine and nanodevices and to study ensuing novel phenomena on the nanoscale. Polyvinylpyrrolidone (PVP) is one suitable polymer surfactant used in our nanoemulsion synthesis, since it is water-soluble, nonionic, nontoxic, and often used in various medical applications.[32] In practice, many studies have focused on the production of nanoparticles by using the polymer as the surfactant, in addition to the stabilizer or capping agent to protect nanoparticles from coagulation or precipitation.[33–37] We have used the polymer to prepare various nanoparticles by the nanoemulsion methodology, including both PVP-coated Fe_3O_4 magnetic nanocrystals and PVP-coated Fe_3O_4–Au core–shell nanoparticles of ultra-small dimension.[33,37] Relevantly, we mention the study on the formation and properties of the FeAu alloy nanostructures of three compositions, $Au_{0.25}Fe_{0.75}$, $Au_{0.5}Fe_{0.5}$, and $Au_{0.75}Fe_{0.25}$, with a narrow particle size distribution by using different surfactants instead of PVP, for instance, the co-surfactants of oleic acid and oleylamine.[28] The nanoparticles have maintained the optical and magnetic properties of the individual constituents and an interesting phenomenon of giant diamagnetism emerges in the case of $Au_{0.5}Fe_{0.5}$.[28,38] In this paper, we report the low-temperature preparation of the PVP–FeAu multifunctional nanoparticles (PVP-coated FeAu multifunctional alloy nanoparticles) by one-step nanoemulsion in the nanoreactor formed by the PVP macromolecules, as shown in the schematic illustration of Fig. 1. The process eliminates the use of the toxic iron carbonyl and introduces the bio-friendly covering of the PVP molecules, which is suitable for further surface modification. The crystal structure and properties of the nanoparticles are thoroughly analyzed in comparison to other related nanoparticles. The characterization shows the PVP coating on the surface of the resultant FeAu nanoparticles and the morphological analysis illustrates the nanoparticle shape, size, and size distribution. In the structural analysis and magneto-plasmonic measurements, the integration of the binary elements into one FeAu nanostructure entity is substantiated, which retains both optical and magnetic properties of the individual components, with well-behaved magnetic response and plasmon resonance. Of interest, the growth habit of the PVP-capped FeAu nanoparticles are compared to that of the PVP-capped Fe_3O_4/Au core–shell nanoparticles and the FeAu nanoparticles prepared from the co-surfactants of oleic acid and oleylamine. Subsequently, a simple, visual demonstration shows that all nanoparticles can effectively be manipulated magnetically, whereas the magnetic hysteresis curves of the nanoparticles are further elucidated by modified bi-phase Langevin equations, which were in turn rationally accounted for by the two components of the particle size distribution.

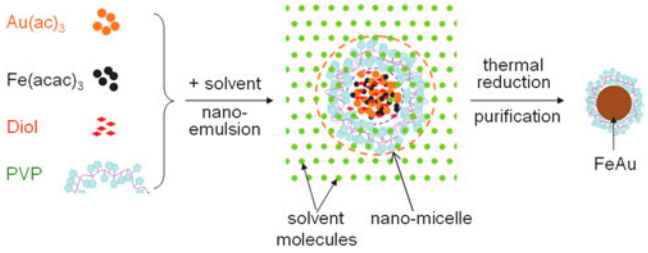


FIG. 1. Schematic route for the growth of the polyvinylpyrrolidone (PVP)-capped FeAu magneto-plasmonic nanoparticles in the nano-micelles formed by the PVP macromolecules.

II. EXPERIMENTAL

A. Chemicals

The two precursors used for the preparation of the FeAu nanoparticles are gold acetate ($Au(ac)_3$, 99.9%) and iron (III) acetylacetonate ($Fe(acac)_3$, 99.9%). Other chemicals include 1,2-hexadecanediol ($C_{14}H_{29}CH(OH)CH_2(OH)$, 90%), poly(vinylpyrrolidone) (PVP, M_w = 55,000), octyl ether ($C_8H_{17}OC_8H_{17}$, 99%), and solvents such as hexane and ethanol. All materials were purchased from Aldrich (Steinheim, Germany) except gold acetate from Alfa Aesar (Ward Hill, MA), and were used as received without further processing.

B. Low-temperature synthesis of PVP-capped FeAu magneto-plasmonic nanoparticles

The PVP-capped FeAu multifunctional nanoparticles (PVP-coated, PVP–FeAu, or polymer–FeAu multifunctional nanoparticles; we use these terms interchangeably) with a nominal ratio of 1:1 were synthesized by one-step nanoemulsion protocols. In the experiment, $Fe(acac)_3$ (0.25 mmol) in 10 mL octyl ether was mixed with $Au(ac)_3$ (0.25 mmol), the reduction agent of 1,2-hexadecanediol (2.5 mmol) and the surfactant of PVP in a 250-mL flask. Under vigorous stirring, the reaction mixture was first heated and homogenized at 80 °C for 1 h to accommodate the formation of the nano-micelles (nanoreactors), then rapidly raised to 280 °C and keep the temperature for 1 h to complete the reaction (Fig. 1). Subsequently, ethanol was added

https://doi.org/10.1557/jmr.2011.161 Published online by Cambridge University Press

to the reacted mixture to precipitate the nanoparticles after cooling down to room temperature. The resulting dark-red product was separated from the supernatant by centrifugation, which was washed with the mixed ethanol/hexane (1:2) several times and re-dispersed in hexane for future use.

C. Structural characterization and measurements of the magneto-plasmonic properties

The morphology, nanoparticle size, and size distribution of the PVP–FeAu magnetic-optical nanoparticles was analyzed by transmission electron microscopy (TEM, JEM-100II and JEOL 2010F), while the crystal structure of the nanoparticles was studied by powder x-ray diffraction (XRD, X'Pert Pro). Vibrating sample magnetometry (VSM, Lakeshore 7300) was applied to perform magnetic measurements on the dried samples to evaluate the magnetic properties of the multifunctional nanoparticles. Furthermore, the optical properties of the samples were characterized by a UV–visible spectrometer (UV–Vis, Hitachi U4100), assessing the surface plasmon resonance characteristic of the nanostructured Au surface. In the Fourier transform infrared spectroscopy (FTIR) investigation, the washed polymer–FeAu nanoparticles and the pure PVP polymer were crushed with a pestle in an agate mortar, separately. The individually crushed material was mixed with potassium bromide (IR spectroscopy grade, Merck, Darmstadt, Germany) in the proportion of ~1:100. The mixture was then compressed into a 2-mm semi-transparent disk by applying a force of 10 tons for 2 min. The FTIR spectra were then recorded in the wave length range of 4000–400 cm^{-1} using an Avatar 360 FTIR spectrometer (Nicolet Company, WI).

D. Magnetic analysis of the hysteresis curves of the PVP–FeAu nanoparticles

Modified Langevin equations were used to analyze the hysteresis curves of the PVP-coated FeAu multifunctional nanoparticles, which were in turn interpreted by the two components of the particle size distribution.

III. RESULTS AND DISCUSSION

A. IR signature of PVP in the PVP–FeAu nanoparticles

As illustrated in Fig. 1, the PVP–FeAu magneto-plasmonic nanoparticles, consisting of the soft shell of the polymer molecules and the hard core of the FeAu multifunctional nanoparticles, were synthesized by the one-step nanoemulsion process in the nanoreactor formed by the PVP molecules.[33,37] The PVP molecules possess remarkable merits such as being water-soluble, non-charged, nontoxic, and often used in various biological and medical applications.[32,37] In our previous researches, the experiments have generated long-term stable, highly crystalline, monosized Fe_3O_4 and Fe_3O_4-Au core–shell nanoparticles using the PVP molecules as the surfactant.[33,37] It has been discovered that a thin PVP layer was actually formed on the surface of the Fe_3O_4 and Fe_3O_4–Au core–shell nanoparticles.[33,37] In consequence, the use of PVP has prospective benefit that delivers a natural layer of such polymer molecules on the surface of the FeAu nanoparticles, potentially useful for surface modification. In this work, PVP plays the role of a surfactant, in addition to the stabilization of the FeAu nanoparticles formed. To ascertain the covering of the PVP macromolecules on the surface of the FeAu nanoparticles to produce the soft shell, FTIR investigation was conducted on the purified product in comparison to the pure polymer. Figure 2 compares the FTIR spectrum of the polymer–FeAu nanosystem after purification with that of the pure PVP molecules used in the synthesis as the surfactant. In Fig. 2(b), the intact PVP molecules show a strong band for the C=O stretching vibration at ~1637.3 cm^{-1} and a sharp band for the C–N stretching vibration at ~1110.8 cm^{-1}.[33,39] These characteristic vibrations reappear in the FTIR spectrum of the polymer–FeAu nanoparticles [Fig. 2(a)], but shifting to the positions of ~1702.1 cm^{-1} for the C=O stretching vibration and ~1289.2 cm^{-1} for the C–N stretching vibration, respectively. In addition, the band shapes and absorption intensities apparently vary considerably from the intact PVP molecules to the polymer–FeAu nanoparticles. The blue-shifting and change in the band shape of the C–N and carbonyl-stretching bands may involve the coordination of the nitrogen and oxygen atoms of the amide group to the Au metallic atoms.[40] In comparison to the PVP molecules on the surface of the Fe_3O_4–Au core–shell nanoparticles, the C=O stretching vibration in the case of the polymer–FeAu nanoparticles shows much stronger blue-shifting, from ~1658.5 cm^{-1} for the former to ~1702.1 cm^{-1} for the latter.[37] The observation suggests

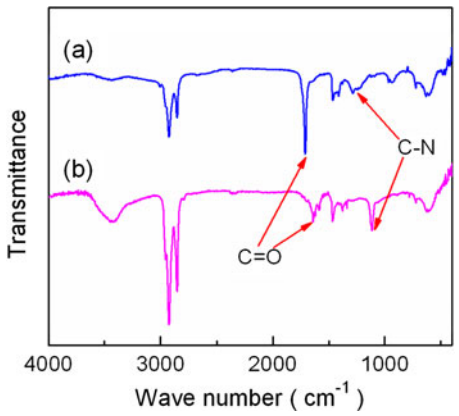


FIG. 2. Fourier transform infrared spectroscopy spectra of (a) the polymer–FeAu nanoparticles and (b) the pure PVP molecules. The C=O and C–N bands are indicated by the respective arrows.

https://doi.org/10.1557/jmr.2011.161 Published online by Cambridge University Press

that in addition to Au, the iron atoms are present on and/or proximate to the surface of the hard core, which may bring about strong interaction with C=O, in contrast to the case of the Fe_3O_4–Au core–shell nanoparticles that permit solely the gold atoms sitting on the surface. The difference in the blue-shifting of the C–N stretching vibration, however, is insignificant in both PVP–FeAu nanoparticles (~1289.2 cm^{-1}) and PVP-coated Fe_3O_4–Au core–shell nanoparticles (~1288.3 cm^{-1}), indicative of similar interactions of the C–N bonding with the surface Au atoms in both cases. As a result, it is evident that as redundant PVP molecules were removed by the washing procedure, the phenomenon explicitly validates the coating of the PVP molecules onto the surface of the FeAu multifunctional nanoparticles to construct a soft shell, which can be further borne out by the other relevant absorption bands in the spectra.

B. Crystal structural analysis of the polymer–FeAu nanoparticles

The crystal structure of the polymer–FeAu nanoparticles as synthesized was recorded by XRD, as shown in Fig. 3(a). As the PVP soft shell is in a noncrystalline state and shows no characteristic diffraction in the range, the diffractions peaking at 38.14°, 44.18°, 64.62°, and 77.70° are properly assigned to the crystalline FeAu core material at the positions of (111), (200), (220), and (311) planes. The evaluation of the diffraction positions gives a crystallographic parameter of 4.074 Å, which is located between the equivalent positions of the corresponding constituent materials (JCPDS Nos. 87-0721 and 04-0784).[26,28] The phenomenon is comparable to the FeAu nanoparticles prepared from the co-surfactants of oleic acid and oleylamine, as shown in Fig. 3(b), in which extra peaks are indicated by the arrows for a possible ordered phase.[28] Of relevance, Fe_3O_4 nanoparticles rather than elemental Fe were obtained if prepared in the same way starting from $Fe(acac)_3$ alone, as shown in Fig. 3(d), in which the diffraction pattern matches the inverse spinel structure of magnetite in bulk (JCPDS No. 88-0315). When they are covered with a thin layer of the Au material, the Fe_3O_4–Au core–shell nanoparticles could be acquired, as shown in Fig. 3(c) in which the extra peaks are ascribed to the cubic structure of gold (JCPDS No. 87-0721), with the diffractions of the Fe_3O_4 core composition indicated by the inverted triangles and showing the concomitant presence of both materials as a result of incomplete shielding of the core by the Au nano-layer.[37] Pure Au nanoparticles were similarly garnered with the single precursor of $Au(OOCCH_3)_3$, showing the same diffraction pattern as the bar diagram in Fig. 3(c). Consequently, the FeAu nanoparticles exist most probably in a compositionally disordered face-centered cubic phase.

The formation of the FeAu crystalline cores are further substantiated by the fact that all the nanoparticles as prepared could be collected by a magnet, leaving no free Au particles visible and thus no co-sedimentation of Fe and Au nanoparticles, as discussed in a next section. Moreover, the average particle size of the FeAu nanoparticles is estimated to be ~13.2 nm based on the full width at half maximum (FWHM) of the (111) peak in Fig. 3(a) by the Scherrer equation, provided that the broadening of the peaks in the XRD pattern is principally attributed to the finite-size of the nanoparticles.[41] The outcome is reasonably in agreement with the TEM analysis below. It is of interest to point out that there is no visible diffraction at ~35.5° that could be associated with the Fe_3O_4 (311) and/or γ-Fe_2O_3 (110) from the possible oxidation of Fe in the polymer–FeAu nanoparticles, which clearly shows the protection function of the PVP macromolecules capped on the surface of the FeAu nanoparticles.

C. Morphology and size monodispersity of the polymer–FeAu nanoparticles

The morphology, nanostructure, particle size, and size distribution of the PVP–FeAu nanoparticles were reorded by TEM. The microimage in Fig. 4(a) shows that the nanoparticles, which are in effect represented by the FeAu part as the polymer layer is transparent to the electron radiation, are rather narrowly spread in the particle size, nearly spherical in shape. The size distribution of the

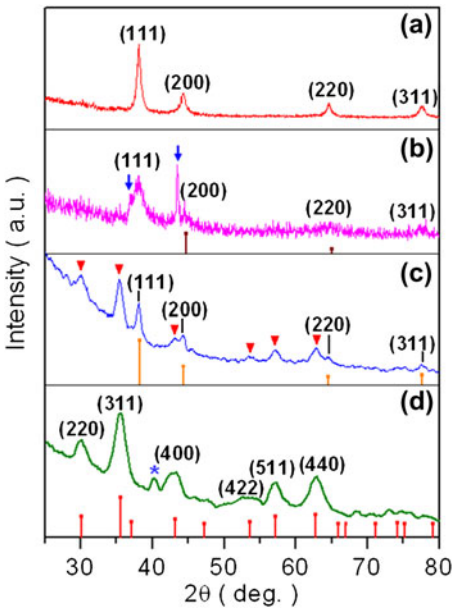


FIG. 3. X-ray diffraction patterns of various nanoparticles. (a) Polymer–FeAu magneto-plasmonic nanoparticles. (b) FeAu nanoparticles prepared from the co-surfactant of oleic acid and oleylamine. Arrows indicate the diffractions of a possible intermetallic phase. Bar diagram for JCPDS of Fe. (c) PVP-coated Fe_3O_4–Au core–shell nanoparticles. Inverted triangles show the peaks of the Fe_3O_4 core. Bar diagram for JCPDS of Au. (d) PVP-coated Fe_3O_4 nanoparticles. Star signs the anomalous Fe_3O_4 (321) reflection. Bar diagram for JCPDS of Fe_3O_4.

https://doi.org/10.1557/jmr.2011.161 Published online by Cambridge University Press

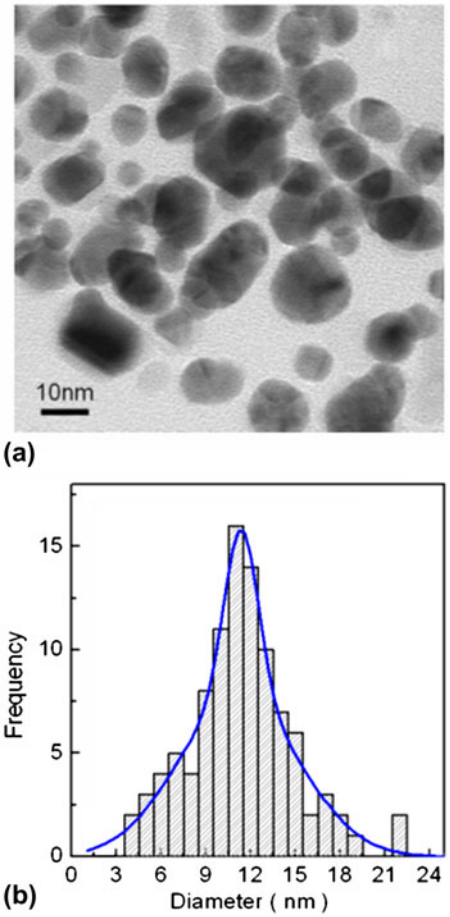


FIG. 4. Transmission electron microscopy morphology and size analysis of the polymer–FeAu magneto-plasmonic nanoparticles. (a) Bright-field image. (b) Histogram of the particle size distribution, with the curve representing the double Gaussian fit.

nanoparticles is given in Fig. 4(b), in which the histogram shows a tight size distribution and has an average size of ~11.3 nm in diameter. As elucidated below, the distribution can be reasonably described by one Gaussian function, but more analysis results in drastic improvement by two Gaussian functions [the curve shown in Fig. 4(b)], which can be exploited to justify the observed magnetic hysteresis curves of the nanosystem.

D. Nanostructural elucidation of the polymer–FeAu nanoparticles

The microstructure of the nanoparticle or precisely its hard core, FeAu nanoparticle, since the polymer layer as mentioned above is effectively transparent to the electron beam, was visualized by high-resolution TEM imaging (HRTEM), compared to other related nanoparticles (Fig. 5). The image of Fig. 5(a) records the lattices of a single FeAu nanoparticle coated by the PVP molecules (i.e., the polymer–FeAu nanoparticle). Evidently, the fringe lattices show the polycrystallinity of the nanoparticle, dividing into the domain nanostructure, which

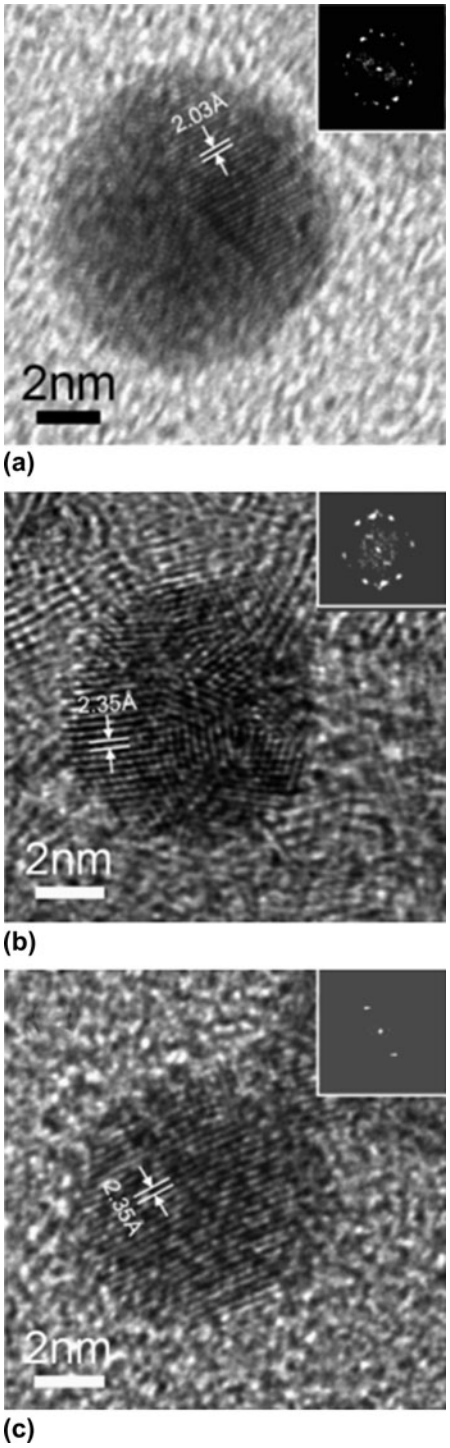


FIG. 5. High-resolution TEM elucidation of the polymer–FeAu magneto-plasmonic nanoparticle and relevant nanoparticles. (a) Lattice image of an individual polymer–FeAu nanoparticle showing the polycrystalline nature with the labeling of the projected (200) plane. Inset: fast Fourier transform (FFT) result of the lattices. (b) Lattice image of a single FeAu nanoparticle prepared from the co-surfactant of oleic acid and oleylamine, exposing the polycrystalline character and the projection of the (111) plane. Inset: FFT result of the lattices. (c) High-resolution image of a single PVP-coated Fe_3O_4–Au core–shell nanoparticle, revealing the monocrystallinity of the Au nano-shell and displaying the projection of the (111) plane. Inset: FFT result of the lattices.

https://doi.org/10.1557/jmr.2011.161 Published online by Cambridge University Press

is further corroborated by the fast Fourier transform (FFT) of the lattice image, as shown in the inset. A representative spacing of the lattices, 2.03 Å, is labeled in the image, which corresponds to the {200} reflection of the FeAu face-centered cubic (fcc) phase as addressed above.[26,28] Crystallographically, the growth habit of FeAu in the nanoparticles is similar to, but more ordered than the FeAu nanoparticles synthesized from the co-surfactant of oleic acid and oleylamine.[28] As shown in Fig. 5(b), the FeAu nanoparticle harvested from the surfactants of oleic acid and oleylamine is composed of nanodomains in the dimension of a few cells, as overtly revealed in the FFT pattern [inset of Fig. 5(b)]. The marker shows the lattice spacing of 2.35 Å for the projection of the (111) atomic arrangement. Strikingly different from the polycrystallinity of the polymer–FeAu nanoparticles and other FeAu nanoparticles from small organic surfactants, the PVP-capped Fe_3O_4–Au core–shell nanoparticle similarly prepared is monocrystalline, as shown in Fig. 5(c). In the image, the highly regular lattices cover the entire nanoparticle, as reaffirmed by the FFT pattern in the inset. It has a lattice spacing of 2.35 Å, representing the projected (111) plane of the Au nano-shell. It is worthy to note that the selected-area electron diffraction (SAED) produces a powder pattern, illustrating the superposition of diffractions of the disoriented FeAu nanoparticles, and useful information of nano-diffraction shall be acquirable in future work from a single nanoparticle to facilitate direct elucidation of the nanoarchitecture of such nanostructures. Nevertheless, the TEM-EDX (energy dispersive x-ray analysis) characterization performed on a single PVP–FeAu nanoparticle shows the concurrent presence of both Fe and Au in it, offering further evidence for the formation of the alloy nanostructure. Overall, the TEM observation provides otherwise no indication of such nanostructures as dendrite or dumbbell, from simply joining separable Au and Fe or Fe_3O_4 nanoparticles.

E. Magnetic properties and analysis of the polymer–FeAu nanoparticle assembly

The magnetic properties of the PVP–FeAu multifunctional nanoparticles were studied by VSM at room temperature, as shown in Fig. 6(a). As the PVP macromolecules are nonmagnetic in essence, direct contribution from the soft shell formed by them is thus negligible and so the magnetism of the nanosystem is dominated by the FeAu ingredient which is in turn protected by PVP from oxidation. Nonetheless, it is useful to note that the PVP capping could have indirect effects on the surface magnetism of the PVP–FeAu nanoparticles which asks for more delicate characterization and precise analysis. In this investigation, the measurement reveals the soft ferromagnetic properties of the nanosystem with a coercivity of ~40 Oe and magnetization of 4.4 emu/g at ~1 T which is still from saturation.[28] This finding is similar to the FeAu

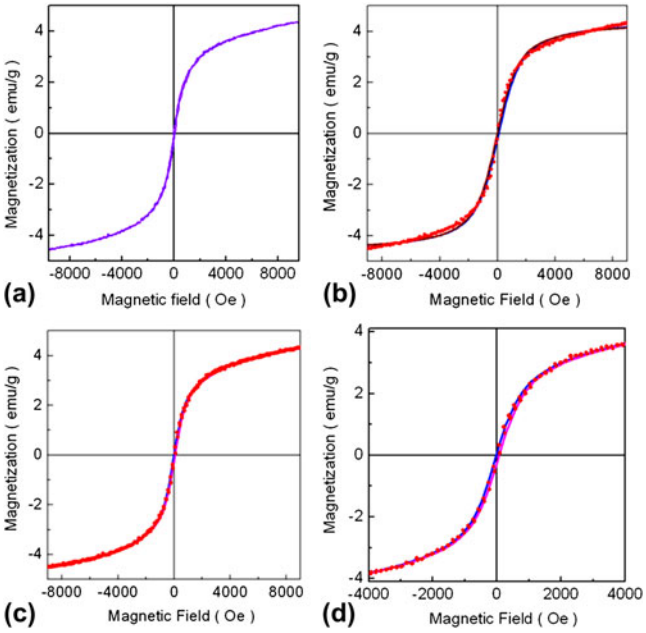


FIG. 6. Magnetic analysis of the polymer–FeAu magneto-plasmonic nanosystem. (a) Hysteresis curve recorded at room temperature. (b) Fit of the hysteresis by the modified single-phase Langevin equations. (c) Resolution of the hysteresis by the modified bi-phase Langevin equations. (d) Expanded plotting of (c) in a narrower range for scrutiny. Experimental data in dots and the fitting results in curves.

nanoparticles of smaller dimension made from different surfactants such as the co-surfactant of oleic acid and oleylamine, but reduced magnetization.[28] Indeed, the magnetic property of the FeAu nanoparticles as a function of dimension is an interesting but intricate issue requiring rigorous treatments. The phenomena observed in Fig. 6(a) is partially interpreted in the microstructural variation due to increased dimension, which could alter the spin-glass behavior in Fe–Au systems, in addition to other factors such as finite-size effects, surface magnetism, induced magnetism in nanostructured Au, spin–spin, and spin–orbital interactions.[42] In effect, the giant diamagnetism was identified in the FeAu nanoparticles of smaller dimension.[38]

The problem of superparamagnetic magnetization has been managed by the Langevin function on an assembly of magnetic nanoparticles with freely rotating moments,[37,43]

$$\frac{M}{M_S} = \coth(\alpha) - \frac{1}{\alpha} \quad , \tag{1}$$

where

$$\alpha = \frac{\mu H}{k_B T} \quad . \tag{2}$$

In the equations, M/M_S is the magnetization normalized to the saturation magnetization, H the applied magnetic field, T the temperature, and k_B is the Boltzmann constant.

https://doi.org/10.1557/jmr.2011.161 Published online by Cambridge University Press

In this work, we are concerned with the PVP–FeAu multifunctional nanoparticles. As the nanoparticles show a soft ferromagnetic behavior, the Langevin function is modified to introduce the setting-in of a coercive field H_c[37,44]

$$\frac{M}{M_s} = \coth(\alpha') - \frac{1}{\alpha'} \quad , \tag{3}$$

with

$$\alpha' = \frac{\mu(H - H_c)}{k_B T} \quad . \tag{4}$$

An initial analysis shows that the data in Fig. 6(a) can be reasonably elucidated by Eq. (3), but deviation is apparent. Or precisely, as given in Fig. 6(b), the data of the PVP–FeAu multifunctional nanoparticle assembly in Fig. 6(a) at the low field can be reasonably elucidated by Eq. (3), or a single-phase fitting, but the discrepancy is noticeable and becomes more severe at the high field. As shown in Fig. 6(c), precise description by a bi-phase superposition of Eq. (3),

$$M = M_s^1\left[\coth(\alpha_1) - \frac{1}{\alpha_1}\right] + M_s^2\left[\coth(\alpha_2) - \frac{1}{\alpha_2}\right] \quad , \tag{5}$$

is achieved, highlighting that the nanosystem most probably consists of two magnetic phases. In the equation, M_S^1, M_S^2, α_1, and α_2 are the fitting quantities corresponding to phase 1 and phase 2, respectively. The fitting excellently extends over the entire range of the measurement, which is expanded in Fig. 6(d) in the narrower range for visibility. Table I sums up the fitting results including the parameters from both down-field and up-field sweepings, where R is the correlation coefficient and $\beta = k_B T/\mu$, in addition to the conventions mentioned above. Within the error of the measurements, the fittings turn out to be rational with high precision. The distinctive feature in the fitting is the switching field β, which is an important parameter in controlling the shape of hysteresis curves. The value of β differs drastically, reading ~315 and ~2810 Oe for the two phases, respectively. In consequence, the analysis compellingly suggests that the PVP–FeAu nanosystem is composed of two magnetic phases.

In the precedent section, the hysteresis curves have been quite well described by the modified bi-phase Langevin equation. In this section, one mechanism leading to the phenomenon is explored in the way of multiple components of the particle size distribution of the nanosystem.[44] In this fashion, the fitting of the particle size distribution by one Gaussian function [Fig. 7(a)] is tested against by two Gaussian functions [Fig. 7(b)] and the outcomes are summarized in Table II, in which R is the correlation coefficient and other symbols are assigned below. As remarked above, the distribution can be satisfactorily fitted by one single Gaussian function, but the deviation is obvious considering the fact that only ~78% of the distribution is tallied even with an offset. In the opposite, the fitting by the two Gaussian functions results in almost perfect description, decomposing the distribution without offsetting in two components of ~77 and 23% each. In Fig. 7(b), the major curve representing the total calculated distribution is the sum of the two minor curves standing for the two calculated component distributions. Both average particle sizes (μ) are almost located at the same positions, 11.2 and 11.4 nm, respectively, which are minute difference from the value of 11.3 nm from the single Gaussian function. However, the parameter of the standard deviation (σ), which reflects the monodispersity of the particle size distribution, changes dramatically from 1.1 to 4.0 nm for the particle size component 1 and 2, correspondingly. It means that the distribution is well split into two particle size components, with one major component and one minor one. We are therefore convinced that the PVP–FeAu nanoparticles are most probably composed of two particle size fractions, and thus give rise in turn to the two distinct magnetic phases, as analyzed above.

TABLE I. Parameters derived from the fitting of the experimental hysteresis curves to the modified single- and bi-phase Langevin equations.

Parameters	Down-field sweep		Up-field sweep	
(a) Single-phase fit				
M_S (emu/g)	4.6 (0.0)		4.6 (0.0)	
H_c (Oe)	−48.5 (9.8)		45.5 (10.0)	
β (Oe)	594.1 (7.5)		606.6 (7.7)	
R^2	0.99847		0.99844	
Offset (emu/g)	−0.1 (0.0)		−0.1 (0.0)	
	Down-field sweep		Up-field sweep	
	Phase 1	Phase 2	Phase 1	Phase 2
(b) Bi-phase fit				
M_S (emu/g)	3.1 (0.0)	2.0 (0.0)	3.1 (0.0)	2.0 (0.0)
H_c (Oe)	−48.5 (2.8)	29.4 (29.5)	42.3 (2.5)	83.6 (28.6)
β (Oe)	311.2 (3.8)	2738.7 (73.7)	319.7 (3.4)	2894.3 (74.0)
R^2	0.99992		0.99993	
Offset (emu/g)	−0.1 (0.0)		−0.1 (0.0)	

Fitting errors in the brackets.

F. Optical properties and magnetic manipulation of the polymer–FeAu magneto-plasmonic nanoparticles

On account of its surface plasmon resonance (SPR), nanostructured Au (e.g., nanoparticles and nanowires) has been studied for its fascinating absorption bands in the visible range, which are subject to the factors of dimension, shape, and physicochemical environment surrounding the Au nanostructure.[15,45] Figure 8 shows the UV–Vis spectra comparing the PVP–FeAu nanoparticles

https://doi.org/10.1557/jmr.2011.161 Published online by Cambridge University Press

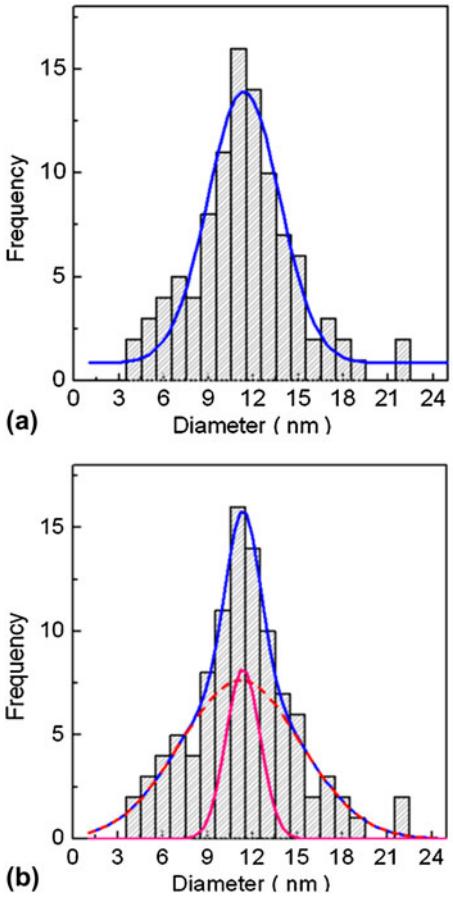


FIG. 7. Analysis of the particle size distribution of the polymer–FeAu magneto-plasmonic nanosystem. (a) Fitting by one Gaussian function and (b) fitting by the sum (major curve) of two Gaussian functions (minor curves). Experimental data in columns and fittings in curves.

TABLE II. Parameters derived from the fitting of the particle size histogram by one and two Gaussian equations, respectively.

Parameters	One Gaussian equation	Two Gaussian equations	
		Component 1	Component 2
μ (nm)	11.3 (0.2)	11.2 (0.3)	11.4 (0.1)
σ (nm)	2.4 (0.2)	4.0 (0.6)	1.1 (0.2)
Fraction (%)	78.5 (6.6)	77.2 (10.1)	23.7 (7.3)
R^2	0.93162	0.97106	
Offset	0.9 (0.4)	0.0 (0.5)	

Fitting errors in the brackets.

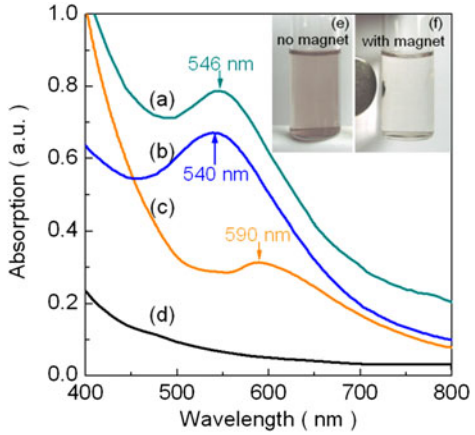


FIG. 8. (a)–(d) UV–Vis absorption spectra of various nanoparticles and (e, f) magnetic manipulation of the polymer–FeAu magneto-plasmonic nanosystem. (a) Polymer–FeAu magneto-plasmonic nanosystem. (b) FeAu nanoparticles prepared from the co-surfactant of oleic acid and oleylamine. (c) PVP-coated Fe_3O_4–Au core–shell nanoparticles. (d) Fe_3O_4 nanoparticles. (e) Violet, homogenous solution of the polymer–FeAu magneto-plasmonic nanosystem in hexane. (f) Clear, transparent solution of the polymer–FeAu magneto-plasmonic nanosystem in hexane after magnetic separation. Arrows in (a)–(c) indicate the respective SPR peak positions.

dispersed in hexane to that of the FeAu (~5.2 nm) from the co-surfactant of oleic acid and oleylamine, PVP-coated Fe_3O_4–Au core–shell nanoparticles (~8 nm) and Fe_3O_4 (~8 nm). The SPR response for the PVP–FeAu nanoparticles shows a well-defined absorption shape with the maximum absorption at the wave length of ~546 nm [Fig. 8(a)], demonstrating the optical property of the FeAu nanostructure coated by PVP. In contrast, the FeAu from the co-surfactant of oleic acid and oleylamine has an absorption peak at ~540 nm [Fig. 8(b)], slightly shorter than that of the PVP–FeAu nanoparticles, though the latter has a much larger particle size (~11.3 nm). Moreover, the PVP-coated Fe_3O_4–Au core–shell nanoparticles manifest a plasmon resonance centered at ~590 nm [Fig. 8(c)].[37] As reported previously, the Au nanoparticles (~8 nm) have the maximum absorption at the wave length of ~525 nm, strongly blue-shifted relative to both kinds of the FeAu nanoparticles.[37] The phenomena clearly prove that at least factors such as dimension, composition, nanostructuring, and dielectric medium are in play and compete with each other.[45] As anticipated, the Fe_3O_4 nanoparticles give no characteristic absorption in the visible range [Fig. 8(d)]. Therefore, the analysis robustly corroborates the formation of the nanoparticles comprising the FeAu core nanoparticles covered by PVP yet again.

We turn to illustrate the functioning of the polymer–FeAu magneto-plasmonic nanoparticles in potential applications, for instance, as nano-reporters, nano-transporters, or nano-actuators.[9,14] As the nano-gold has the plasmon resonance absorption for accurate optical sensing [Fig. 8(a)], the soft ferromagnetic character of the nanoparticles [Fig. 6(a)] facilitates rapid, efficient manipulation. Figures 8(e) and 8(f) visually demonstrate a separation and redispersion process of the nanoparticles in hexane. Under the influence of an external magnetic field, the coated magnetic-optical nanoparticles change from a violet, homogeneous dispersion [Fig. 8(e)] to a clear, transparent solution after the nanoparticles being collected by a magnetic

https://doi.org/10.1557/jmr.2011.161 Published online by Cambridge University Press

disk [Fig. 8(f)]. The collected nanoparticles can be reversibly dispersed by agitation after removal of the magnetic field and the above process can be repeated. The color of the solution in Fig. 8(e) is complementary to the corresponding UV–Vis absorption of Fig. 8(a). Hence, the finding excludes the possibility of separate Au and Fe or Fe_3O_4 nanoparticles in the preparation of the polymer–FeAu nanoparticles and sustains the nanostructuring of the FeAu nanoparticles. In the experiment, such a process was not observed in the case of a mixture from the separate Fe_3O_4 and Au deliberately mixed together. Resultantly, the construction of the FeAu nanoparticles are once again authenticated by the observation as all PVP-coated FeAu nanoparticles as prepared could be collected by a magnet [Fig. 8(f)], showing no free Au nanoparticles and co-sedimentation of Au and Fe or Fe_3O_4 nanoparticles (possible nanostructures from sticking Au and Fe or Fe_3O_4 together, such as dendrite or dumbbell, have been decisively ruled out in the TEM analysis above). Of interest, we state that owing to the Au atoms on the surface of the FeAu nanoparticles, the PVP–FeAu nanoparticles prepared by the one-step nanoemulsion are capable of being rendered for biomedical applications through ready linkage to other molecules containing mercapto functional groups, executing optical detection, photonic therapy, magnetic separation, manipulation, and actuation under an external magnetic field.[3,28]

Finally, we briefly comment that the FeAu nanoparticle size may be controllable by adjusting the experimental conditions, such as the amounts of the surfactant and/or the precursors.[46] Of significance, the composition different from $Fe_{0.5}Au_{0.5}$ is also obtainable through changing the ratio of the precursors.[28] So, the structure and properties of such nano-entities, particularly with respect to magnetic, optical, and surface characteristics, could be modified correspondingly.[26,28]

IV. CONCLUSIONS

We have synthesized the multifunctional PVP-capped FeAu nanoparticles (FeAu alloy nanoparticles coated by PVP) during the low-temperature one-step nanoemulsion process completed in the nanoreactor formed by the PVP molecules. The nanoparticles, comprising FeAu as the hard core and PVP as the soft shell, take advantages of both magnetic and optical properties in addition to the biological compatibility and benign surface chemistry offered by the compositions. The FTIR study establishes the PVP molecules present on the surface of the nanoparticles. In comparison to the growth habits of other related nanoparticles, the structural analysis of the nanoparticles verifies the formation of the FeAu alloy nanocores of ~11.3 nm in diameter with a narrow particle size distribution. Moreover, the magnetic measurement shows the soft ferromagnetic behavior of the nanoparticles with a small coercivity of ~40 Oe at room temperature. The relevant magnetic hysteresis curves were subsequently explicated by the modified bi-phase Langevin equations, probably resulting from the binary components of the particle size distribution. The optical property of the nanosystem was determined by the UV–Vis measurements, revealing a well-behaved surface plasmon absorption band located at ~546 nm, and a visual demonstration shows that all nanoparticles are magnetically separable for manipulation of interest. The characterization, thus, proves the integration of the optical functionality of Au and the magnetic properties of iron into the FeAu core, which is covered and protected by the biocompatible PVP molecules. Such nanoparticles promise potential niche applications such as optical sensing, photonic therapy, magnetic sorting and drug delivery.

ACKNOWLEDGMENTS

This work was supported in part by the Scientific and Technological Development Projects, Science and Technology Department of Henan Province, China (Nos. 092102210004 and 092300410031, and 11230040011), the Natural Science Research Foundation Grants, Education Department of Henan Province, China (Nos. 2009A150004 and 2009A150005), the Pioneer Research Center Program through the National Research Foundation of Korea funded by the Ministry of Education, Science and Technology, South Korea (No. 2010-0002190), and the Industrial Core Technology Development Program funded by the Ministry of Knowledge Economy, South Korea (No. 10033183).

REFERENCES

1. A.S. Arico, P. Bruce, B. Scrosati, J-M. Tarascon, and W. Schalkwijk: Nanostructured materials for advanced energy conversion and storage devices. *Nat. Mater.* **4**, 366 (2005).
2. C. Ross: Patterned magnetic recording media. *Annu. Rev. Mater. Res.* **31**, 203 (2001).
3. H.L. Liu, C.H. Sonn, J.H. Wu, K.M. Lee, and Y.K. Kim: Synthesis of streptavidin-FITC-conjugated core–shell Fe_3O_4-Au nanocrystals and their application for the purification of $CD4^+$ lymphocytes. *Biomaterials* **29**, 4003 (2008).
4. P. Li, D.E. Miser, S. Rabiei, R.T. Yadav, and M.R. Hajaligol: The removal of carbon monoxide by iron oxide nanoparticles. *Appl. Catal. B* **43**, 151 (2003).
5. S. Kim, J. Lim, S. Lee, C. Heo, and S. Yang: Biofunctional colloids and their assemblies. *Soft Matter.* **6**, 1092 (2010).
6. S. Hockfield: The next innovation revolution. *Science* **323**, 1147 (2009).
7. Y. Ji, S. Yang, S. Guo, X. Song, B. Ding, and Z. Yang: Bimetallic Ag/Au nanoparticles: A low temperature ripening strategy in aqueous solution. *Colloids Surf. A* **372**, 204 (2010).
8. B.I. Kharisov, O.V. Kharissova, M.J. Yacaman, and U.O. Mendez: State of the art of the bi- and trimetallic nanoparticles on the basis of gold and iron. *Recent Pat. Nanotechnol.* **3**, 81 (2009).
9. A.G. Roca, R. Costo, A.F. Rebolledo, S. Veintemillas-Verdaguer, P. Tartaj, T. Gonzalez-Carreno, M.P. Morales, and C.J. Serna: Progress in the preparation of magnetic nanoparticles for applications in biomedicine. *J. Phys. D: Appl. Phys.* **42**, 224002 (1–11) (2009).

https://doi.org/10.1557/jmr.2011.161 Published online by Cambridge University Press

10. G. Glockl, R. Hergt, M. Zeisberger, S. Dutz, S. Nagel, and W. Weitschies: The effect of field parameters, nanoparticle properties and immobilization on the specific heating power in magnetic particle hyperthermia. *J. Phys. Condens. Matter.* **18**, S2935 (2006).
11. M. Wakisaka, H. Suzuki, S. Mitsui, H. Uchida, and M. Watanabe: Increased oxygen coverage at Pt-Fe alloy cathode for the enhanced oxygen reduction reaction studied by EC−XPS. *J. Phys. Chem. C* **112**, 2750 (2008).
12. Y.W. Wang, L.D. Zhang, G.W. Meng, X.S. Peng, Y.X. Jin, and J. Zhang: Fabrication of ordered ferromagnetic-nonmagnetic alloy nanowire arrays and their magnetic property dependence on annealing temperature. *J. Phys. Chem. B* **106**, 2502 (2002).
13. H. Li, K.M. Liew, X.Q. Zhang, J.X. Zhang, X.F. Liu, and X.F. Bian: Electron-conduction properties of Fe-Al alloy nanowires. *J. Phys. Chem. B* **112**, 15588 (2008).
14. M-C. Daniel and D. Astruc: Gold nanoparticles: Assembly, supramolecular chemistry, quantum-size-related properties, and applications toward biology, catalysis, and nanotechnology. *Chem. Rev.* **104**, 293 (2004).
15. S. Link, M.B. Mohamed, and M.A. El-Sayed: Simulation of the optical absorption spectra of gold nanorods as a function of their aspect ratio and the effect of the medium dielectric constant. *J. Phys. Chem. B* **103**, 3073 (1999).
16. Y. Lu, C. Shi, M-J. Hu, Y-J. Xu, L. Yu, L-P. Wen, Y. Zhao, W-P. Xu, and S-H. Yu: Magnetic alloy nanorings loaded with gold nanoparticles: Synthesis and applications as multimodal imaging contrast agents. *Adv. Funct. Mater.* **20**, 3701 (2010).
17. L.B. Scaffardi, N. Pellegri, O. de Sanctis, and J.O. Tocho: Sizing gold nanoparticles by optical extinction spectroscopy. *Nanotechnology* **16**, 158 (2005).
18. J.F. Hainfeld and R.D. Powell: New frontiers in gold labeling. *J. Histochem. Cytochem.* **48**, 471 (2000).
19. Y.W. Lee, N.H. Kim, K.Y. Lee, K. Kwon, M. Kim, and S.W. Han: Synthesis and characterization of flower-shaped porous Au-Pd alloy nanoparticles. *J. Phys. Chem. C* **112**, 6717 (2008).
20. X. Zhang, M. Tsuji, S. Lim, N. Miyamae, M. Nishio, S. Hikino, and M. Umezu: Synthesis and growth mechanism of pentagonal bipyramid-shaped gold-rich Au/Ag alloy nanoparticles. *Langmuir* **23**, 6372 (2007).
21. A.M. Molenbroek and J.K.N.B.S. Clausen: Structure and reactivity of Ni-Au nanoparticle catalysts. *J. Phys. Chem. B* **105**, 5450 (2001).
22. D.L. Lu, K. Domen, and K.I. Tanaka: Electrodeposited Au-Fe, Au-Ni, and Au-Co alloy nanoparticles from aqueous electrolytes. *Langmuir* **18**, 3226 (2002).
23. J.B. Xu, T.S. Zhao, Z.X. Liang, and L.D. Zhu: Facile preparation of AuPt alloy nanoparticles from organometallic complex precursor. *Chem. Mater.* **20**, 1688 (2008).
24. H. Okamoto, T.B. Massalski, L.J. Swartzendruber, and P.A. Beck: The Au-Fe (gold-iron) system. *Bull. Alloy Phase Diagrams* **5**, 592 (1984).
25. T.B. Massalski: *Binary Alloys Phase Diagrams*, vol. 1, 2nd ed. (ASM International, Materials Park, OH, 1990) pp. 367–369.
26. I.C. Chiang and D.H. Chen: Synthesis of monodisperse FeAu nanoparticles with tunable magnetic and optical properties. *Adv. Funct. Mater.* **17**, 1311 (2007).
27. N. Dahal, V.C.J. Jasinski, and V.J. Leppert: Synthesis of water-soluble iron-gold alloy nanoparticles. *Chem. Mater.* **20**, 6389 (2008).
28. H.L. Liu, J.H. Wu, J.H. Min, and Y.K. Kim: Synthesis of monosized magnetic-optical AuFe alloy nanoparticles. *J. Appl. Phys.* **103**, 07D529 (1–3) (2008).
29. G. Albanese, A. Deriu, J. Moya, E. Angeli, D. Bisero, A. Da Re, F. Ronconi, F. Spizzo, P. Vavassori, M. Baricco, and E. Bosco: Mossbauer investigation of Au/Fe alloys with giant magnetoresistence properties. *J. Magn. Magn. Mater.* **272–276**, 1545 (2004).
30. Z.H. Ban, Y.A. Barnakov, V.O. Golub, and C.J. O'Connor: The synthesis of core-shell iron@gold nanoparticles and their characterization. *J. Mater. Chem.* **15**, 4660 (2005).
31. K. Sato, B. Bian, and Y. Hirotsu: $L1_0$ type ordered phase formation in Fe–Au nanoparticles. *Jpn. J. Appl. Phys.* **41**(Part 2), L1 (2002).
32. F. Fischer and S. Bauer: Polyvinylpyrrolidon: A versatile substance in chemistry. *Chemistry in our Time.* **43**, 376 (2009).
33. H.L. Liu, S.P. Ko, J.H. Wu, M.H. Jung, J.H. Min, J.H. Lee, B.H. An, and Y.K. Kim: One-pot polyol synthesis of monosize PVP-coated sub-5nm Fe_3O_4 nanoparticles for biomedical applications. *J. Magn. Magn. Mater.* **310**, e815 (2007).
34. H. Huang, Q. Xie, M. Kang, B. Zhang, H. Zhang, J. Chen, C. Zhai, D. Yang, B. Jiang, and Y. Wu: Labeling transplanted mice islet with polyvinylpyrrolidone coated superparamagnetic iron oxide nanoparticles for in vivo detection by magnetic resonance imaging. *Nanotechnology* **20**, 365101 (1–9) (2009).
35. H. Shao, Y. Huang, H.S. Lee, Y.J. Suh, and C.O. Kim: Effect of PVP on the morphology of cobalt nanoparticles prepared by thermal decomposition of cobalt acetate. *Curr. Appl. Phys.* **6**, e195 (2006).
36. I. Pardinas-Blanco, C.E. Hoppe, Y. Pineiro-Redondo, M.A. Lopez-Quintela, and J. Rivas: Formation of gold branched plates in diluted solutions of poly(vinylpyrrolidone) and their use for the fabrication of near-infrared-absorbing films and coatings. *Langmuir* **24**, 983 (2008).
37. H.L. Liu, P. Hou, W.X. Zhang, and J.H. Wu: Synthesis of monosized core–shell Fe_3O_4/Au multifunctional nanoparticles by PVP-assisted nanoemulsion process. *Colloids Surf. A* **356**, 21 (2010).
38. J.H. Wu, J.H. Min, H.L. Liu, J.U. Cho, and Y.K. Kim: Giant diamagnetism in AuFe nanoparticles. *IEEE Trans. Magn.* **45**, 2442 (2009).
39. N. Sahiner, N. Pekel, and O. Guven: Radiation synthesis, characterization and amidoximation of N-vinyl-2-pyrrolidone/acrylonitrile interpenetrating polymer networks. *React. Funct. Polym.* **39**, 139 (1999).
40. K. Nakamoto: *Infrared and Raman Spectra of Inorganic and Coordination Complexes* (Wiley, New York, 1978).
41. B.D. Cullity and S.R. Stock: *Elements of X-ray Diffraction* (Prentice Hall, Upper Saddle River, 2001).
42. P. Crespo, R. Litran, T.C. Rojas, M. Multigner, J.M. de la Fuente, J.C. Sanchez-Lopez, M.A. Garcia, A. Hernando, S. Penades, and A. Fernandez: Permanent magnetism, magnetic anisotropy, and hysteresis of thiol-capped gold nanoparticles. *Phys. Rev. Lett.* **93**, 087204 (1–4) (2004).
43. C. Petit and M.P. Pilen: Physical properties of self-assembled nanosized cobalt particles. *Appl. Surf. Sci.* **162/163**, 519 (2000).
44. J.H. Wu: Design and structural characterization of perpendicular magnetic superlattices. *Nanotechnology* **13**, 720 (2002).
45. K.A. Willets and R.P.V. Duyne: Localized surface plasmon resonance spectroscopy and sensing. *Annu. Rev. Phys. Chem.* **58**, 267 (2007).
46. J. Jeong, J.H. Min, A.-Y. Song, J.S. Lee, J.-S. Ju, J.H. Wu, and Y.K. Kim: Nonaqueous synthesis and magnetic properties of $ZnFe_2O_4$ nanocrystals with narrow size distributions. *J. Appl. Phys.* **109**, 07B511(1–3) (2011).

https://doi.org/10.1557/jmr.2011.161 Published online by Cambridge University Press